

Compliant Leg Architectures and a Linear Control Strategy for the Stable Running of Planar Biped Robots

Regular Paper

Behnam Dadashzadeh^{1,2,*}, M.J. Mahjoob², M. Nikkhah Bahrami² and Chris Macnab¹

¹ Department of Electrical and Computer Engineering, University of Calgary, Canada

² School of Mechanical Engineering, University of Tehran, Iran

* Corresponding author E-mail: bdzadeh@ut.ac.ir

Received 15 Mar 2012; Accepted 03 Jul 2013

DOI: 10.5772/56806

© 2013 Dadashzadeh et al.; licensee InTech. This is an open access article distributed under the terms of the Creative Commons Attribution License (<http://creativecommons.org/licenses/by/3.0>), which permits unrestricted use, distribution, and reproduction in any medium, provided the original work is properly cited.

Abstract This paper investigates two fundamental structures for biped robots and a control strategy to achieve stable biped running. The first biped structure contains straight legs with telescopic springs, and the second one contains knees with compliant elements in parallel with the motors. With both configurations we can use a standard linear discrete-time state-feedback control strategy to achieve an active periodic stable biped running gait, using the Poincare map of one complete step to produce the discrete-time model. In this case, the Poincare map describes an open-loop system with an unstable equilibrium, requiring a closed-loop control for stabilization. The discretization contains a stance phase, a flight phase and a touch-down. In the first approach, the control signals remain constant during each phase, while in the second approach both phases are discretized into a number of constant-torque intervals, so that its formulation can be applied easily to stabilize any active biped running gait. Simulation results with both the straight-legged and the kneed biped model demonstrate stable gaits on both horizontal and inclined surfaces.

Keywords Gait Generation, Planar Bipedal Running Control, Poincare Map Fixed Point, State Feedback

1. Introduction

Many researchers have investigated biped robot walking in both theory and practice (see survey in [1]), yet many open problems remain. A mechanical leg lacks the complexity of actuation and sensing of a human leg; thus, the physical design remains an area of investigation. A useful mechanism should be simple, robust and energy efficient. The design of an appropriate control system provides another challenge; the problem is highly nonlinear, open-loop unstable, and constrained by limited actuator power. Moreover, compliant elements that store and release energy (possibly essential for energy efficiency) result in complex dynamics requiring non-trivial control strategies. Contributions to this work include proposing a mechanism - a simple, efficient, and compliant biped - as well as demonstrating the applicability of linear control strategies.

Our understanding of efficient biped walking mechanics and dynamics has improved tremendously through the investigation of passive walkers ([2],[3],[4]) and recently the idea has been successfully extended to passive biped running [5]. Although passive robots can teach us a lot, practical robots need actuation. Two of the most important fully actuated robots are the new generation of Asimo humanoid that can run at 9 km/h [6] and the HRP-2LR biped that can walk and run on level ground, with the running pattern obtained using resolved the momentum control method and the ZMP concept [8]. However, these running motions include very short flight phases and do not come near the efficiency of human running [7] - perhaps because they lack (the efficient use of) compliant elements. The simplest compliant biped model - a spring loaded inverted pendulum - consists of a point mass and two massless springy legs [9], which produces similar ground reaction forces to those found in human walking and running [10]. It has been shown through both simulation and experiments that a compliant leg structure (with linear springs representing biarticular muscle tendons), with simple open-loop sinusoidal motor inputs, can produce natural ground reaction forces for a one-legged hopper [11] and a biped running robot [12]. The elastic coupling of limbs may make gaits faster and more human-like [13]. In order to achieve human-muscle characteristics, some have proposed using artificial pneumatic muscles [14], [15] and others have suggested series elastic actuators [16], [17].

Underactuated biped robots exhibit faster and more natural walking and running gaits [18]. McGeer [19] realized stable and unstable passive running gaits for his biped model with telescoping springy legs and massless arced feet, and stabilized unstable passive gaits with event-based LQR control on its linearized Poincare map. While biped models with arced feet have some stable passive running gaits, no multi-body biped model with point feet has been found to have a stable passive running gait. Hyon et al. [22] proposed a controller based upon an energy preservation strategy for a one legged hopping robot and then applied it to a planar biped robot with springy legs and a torso. Hu et al. [23] investigated unstable passive running gaits for a telescoping springy biped model with massless point feet, and stabilized them using event-based LQR control similar to McGeer [19]. These works were confined to biped models with massless springy legs on horizontal terrain that have passive running gaits, and could not be applied to real biped robot models that do not have a passive limit cycle. Hybrid zero dynamics (HZD) have been used to prove the existence and stability of active bipedal walking [20] and running [21] gaits for a five link four actuator kneed model. A reduced-order hybrid subsystem is used to design the controller.

Our original contributions include making the Poincare map event-based control more general by developing active (rather than just passive) maps of running gaits, which has allowed us to extend the applications to different types of robots running on horizontal and sloped terrains. Also, we generalize this control strategy for active running gaits with variable discretized control commands. Inspired by [23], [12] and [21], we choose two types of biped models to generate running gaits and stabilize them with the proposed control strategy for active gaits. The first system is a straight-legged telescoping springs biped with one active revolute joint at the hip while a second one has three joints at the hip and knees with motors parallel to a torsional spring in each revolute joint. The proposed multi-body biped models can generate running gaits even with simple constant control commands during each phase, which could be very interesting for this complicated task.

2. Dynamic Modelling

2.1 Straight-legged biped

We first investigate a biped with a hip and two prismatic spring legs (illustrated in a with parameters given in Table 1). We assume that a lower piston fits into an upper cylinder on each leg (with a spring in between). Points A and F are the robot's point feet (massless), C and D are the centres of mass (CoMs) of the cylinders, B and E are the CoMs of the respective pistons, and H is the hip point (with a point mass). We assume that the terrain slopes at a constant angle φ and our Cartesian X, Y coordinates describe absolute horizontal and vertical directions (relative to the Earth). We look only at running gaits, consisting of a stance phase (with one stance leg touching the ground and one swing leg) and a flight phase. A rotational motor in the hip provides actuation torque u . The prismatic joints are assumed to have actuators that can only lock or unlock the prismatic motion - locked just after take-off (once the leg has reached its nominal length) and unlocked just before, or at, touch-down. Thus, the prismatic joints are passive.

2.1.1 Stance phase

The generalized coordinates of the stance phase q_s have q_1 as the angle of the stance leg with respect to vertical q_2 as the angle of the swing leg with respect to the stance leg, and q_3 as the length of the stance leg spring. The swing leg (quickly) shortens by length s just after touch-down, and moves (quickly) back to the original length just after take-off.

The Lagrange method results in dynamic equations:

Parameter	Value (SI units)	Description
a	0.15	CH=DH, the distance between the CoM of the cylinder and the hip
b	0.1	AB=EF, the distance between the CoM of the piston and the hip
l_c	0.2	The free length of the spring (length of cylinder)
l_p	0.2	The length of the piston
s	$0.8l_c$	Length of the swing leg to ensure clearance
m_c	2	Mass of the cylinder
m_p	0	Mass of the piston
m_h	3	Point mass of the hip at H
I_c	0.0067	Moment of inertia of the cylinder around the CoM
I_p	0	Moment of inertia of the piston around the CoM
K_s	1000	Leg spring rate
φ	arbitrary	Terrain slope with respect to the horizon
u	variable	Torque of the hip motor exerted between the two legs in the direction of θ_2

Table 1. Nomenclature of the prismatic leg biped robot

$$\frac{d}{dt} \left(\frac{\partial L}{\partial \dot{q}_i} \right) - \frac{\partial L}{\partial q_i} = Q_i \quad (1)$$

in which the Lagrangian function $L(\mathbf{q}, \dot{\mathbf{q}}) = T(\mathbf{q}, \dot{\mathbf{q}}) - V(\mathbf{q})$ is the subtraction of the kinetic and potential energy. The kinetic energy consists of the links' translational and rotational energies, and the potential energy comprises the gravitational and elastic energies. The joints are assumed to be frictionless. The generalized forces Q_i are found using virtual work:

$$\begin{aligned} \delta W &= \sum Q_i \delta q_i \Rightarrow u \delta q_2 = \sum Q_i \delta q_i \\ &\Rightarrow Q_1 = 0, Q_2 = u, Q_3 = 0 \end{aligned}$$

The kinetic and potential energies follow from the geometric relationships between the positions of the robot points and their symbolic time derivatives. The governing equations of the stance phase, derived by symbolic software, are:

$$[\mathbf{D}_s(\mathbf{q}_s)]_{3 \times 3} \cdot [\ddot{\mathbf{q}}_s]_{3 \times 1} + [\mathbf{C}_s(\mathbf{q}_s, \dot{\mathbf{q}}_s)]_{3 \times 1} = [\mathbf{B}_s]_{3 \times 1} u_s \quad (2)$$

in which, $\mathbf{B}_s = [0 \ 1 \ 0]^T$. $\mathbf{D}_s(\mathbf{q}_s)$ is the inertia matrix and $\mathbf{C}_s(\mathbf{q}_s, \dot{\mathbf{q}}_s)$ contains Coriolis, gravity and elastic forces. We do not need to factor multipliers of $\dot{\mathbf{q}}_s$ in $\mathbf{C}_s(\mathbf{q}_s, \dot{\mathbf{q}}_s)$, neither to solve the equations nor to design the controller. Defining the stance phase state vector $\mathbf{x}_s = [\mathbf{q}_s; \dot{\mathbf{q}}_s]$ gives a set of first-order state equations:

$$\dot{\mathbf{x}}_s = \mathbf{f}_s(\mathbf{x}_s) + \mathbf{g}_s(\mathbf{x}_s) \cdot u \quad (3)$$

in which:

$$\mathbf{f}_s(\mathbf{x}_s) = \begin{bmatrix} \dot{\mathbf{q}}_s(\mathbf{x}_s) \\ -\mathbf{D}_s^{-1}(\mathbf{x}_s) \cdot \mathbf{C}_s(\mathbf{x}_s) \end{bmatrix}, \mathbf{g}_s(\mathbf{x}_s) = \begin{bmatrix} \mathbf{0}_{3 \times 1} \\ \mathbf{D}_s^{-1}(\mathbf{x}_s) \cdot \mathbf{B}_s \end{bmatrix}$$

More details about the dynamic equations can be found in [29].

2.1.2 Take-off

A take-off event consists of an instantaneous transition from stance to flight, occurring when the ground reaction force reaches zero. This event is detected when the spring of the stance leg reaches its free length or the ground reaction force reaches zero. The generalized coordinates \mathbf{q}_f in flight use the same q_1 and q_2 as in stance, but include q_3 and q_4 as the Cartesian X and Y coordinates of the hip point respectively. In order to find the initial coordinates in the subsequent flight phase, we use:

$$\begin{aligned} q_{f1}^+ &= q_{s1}^-(t), q_{f2}^+ = q_{s2}^-(t), \\ q_{f3}^+ &= x_H(\mathbf{q}_s^-), q_{f4}^+ = y_H(\mathbf{q}_s^-) \end{aligned} \quad (4)$$

where subscripts s and f represent stance and flight respectively, and superscripts $-$ and $+$ indicate time instants just before and after the event, respectively, which results in:

$$\mathbf{x}_{f, \text{initial}} = \left[q_{f1}^+, q_{f2}^+, q_{f3}^+, q_{f4}^+, \frac{d}{dt} q_{f1}^+, \frac{d}{dt} q_{f2}^+, \frac{d}{dt} q_{f3}^+, \frac{d}{dt} q_{f4}^+ \right]$$

2.1.3. Flight phase

The generalized coordinates of the flight phase \mathbf{q}_f have 4 components, where q_1, q_2 are the same as in the stance phase and q_3, q_4 indicate the position of the hip point. The generalized forces during the flight phase are $Q_1 = 0, Q_2 = u, Q_3 = 0, Q_4 = 0$.

Assuming that the lengths of the legs are constant during flight, the dynamic equations of flight become:

$$[\mathbf{D}_f(\mathbf{q}_f)]_{4 \times 4} \cdot [\ddot{\mathbf{q}}_f]_{4 \times 1} + [\mathbf{C}_f(\mathbf{q}_f, \dot{\mathbf{q}}_f)]_{4 \times 1} = [\mathbf{B}_f]_{4 \times 1} u_f \quad (5)$$

with $\mathbf{B}_f = [0 \ 1 \ 0 \ 0]^T$.

2.1.4. Touch-down

To detect a touch-down event during numerical simulation, we have to find the first intersection of the trajectory of foot point D and the line $y = x \tan \varphi$. At touch-down, the velocities change instantaneously because of an inelastic impact. The angles do not have any instantaneous change, but our coordinate notation

does change due to the other leg becoming the stance leg (b):

$$\begin{bmatrix} q_{s1}^+ \\ q_{s2}^+ \\ q_{s3}^+ \end{bmatrix} = \begin{bmatrix} q_{f1}^- + q_{f2}^- \\ -q_{f2}^- \\ b_0 \end{bmatrix} \quad (6)$$

We have to utilize the conservation of angular and linear momentum in order to describe the impact map. We assume leg AH has a fixed length during the impact, whereas leg FH is free to compact (compressing the spring). Assuming a fully plastic contact, point F becomes an ideal pivot after contact.

Foot F receives an impulse force, one component of which is transferred along the axis of the prismatic joint to the hip. Using angular momentum conservation for the whole robot around F, linear momentum conservation of AHD in the direction of leg FH, and angular momentum conservation of leg AH around H, then the expressions below are conserved in terms of $\dot{\mathbf{q}}_f^-$ and $\dot{\mathbf{q}}_s^+$:

$$H_F^{AHF}(\dot{\mathbf{q}}_f^-) = H_F^{AHF}(\dot{\mathbf{q}}_s^+) \quad (7)$$

$$L_{FH}^{AHD}(\dot{\mathbf{q}}_f^-) = L_{FH}^{AHD}(\dot{\mathbf{q}}_s^+) \quad (8)$$

$$H_H^{AH}(\dot{\mathbf{q}}_f^-) = H_H^{AH}(\dot{\mathbf{q}}_s^+) \quad (9)$$

where L denotes the linear momentum and H denotes the angular momentum. The three equations (7-9) have three unknowns $\dot{\mathbf{q}}_s^+$, providing a re-initialization of velocities.

Equations (2, 4, 5, 6-9) constitute the overall hybrid dynamic model of running.

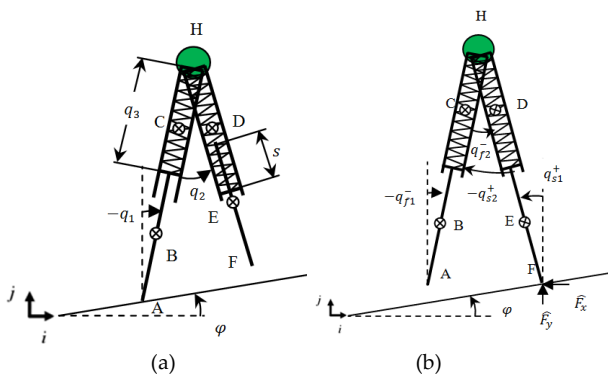


Figure 1. (a) Stance phase generalized coordinates and (b) Touch-down parameters for the straight leg biped

2.2. Kneed biped

Studies on the energetics and kinematics of a spring-mass model show that compliant elements in the legs of a biped robot take an important role in both walking and

running [12]. Although human legs have very complicated muscle-tendon neural control systems, they exhibit simple spring-like behaviour in running and some walking speeds [24]. A one-legged hopper with a springy passive knee achieves a stable hopping motion using a harmonic input for the hip motor [11]. To model a human-like compliant leg, we can use Hill-type muscles in the biped model, but it makes the model unnecessarily complicated. In order to simulate muscle compliance with a minimalistic model, we propose a biped model in which each joint comes equipped with a rotational spring parallel to a torque motor.

This model (Figure 2) consists of a point mass in the hip and two legs with a thigh and a shank, both of which have mass and moment of inertia. The model's lengths and masses model a typical human (). Inspired by the fact that human muscles change their stiffness during running [25], we discovered that changing the knee stiffness between stance and flight produces more efficient running gaits – the gait requires more torque in stance than in flight. We define the free angles of the torsion springs in B and D as $q_2 = -\pi/4$, $q_4 = -\pi/4$, and the free angle of the hip torsion spring as $q_3 - q_1 = 0$. The procedure in section 2-4 remains valid for this model.

The stance phase's generalized coordinates comprises q_1 (the absolute angle of thigh BH), q_2 (the angle of link AB relative to BH), q_3 (the absolute angle of thigh DH) and q_4 (the angle of link CD relative to DH), as shown in Figure 2a. The positive direction of the angles is counter-clockwise. By utilizing the Lagrange method, the stance phase dynamic equations become:

$$[\mathbf{D}_s(q_s)]_{4 \times 4} \cdot [\ddot{\mathbf{q}}_s]_{4 \times 1} + [\mathbf{C}_s(q_s, \dot{q}_s)]_{4 \times 1} = [\mathbf{B}_s]_{4 \times 3} \cdot [\mathbf{u}_s]_{3 \times 1} \quad (10)$$

in which, $\mathbf{B}_s = \begin{bmatrix} -1 & 0 & 0 \\ 0 & 1 & 0 \\ 1 & 0 & 0 \\ 0 & 0 & 1 \end{bmatrix}$, $\mathbf{u} = \begin{bmatrix} u_1 \\ u_2 \\ u_3 \end{bmatrix}$.

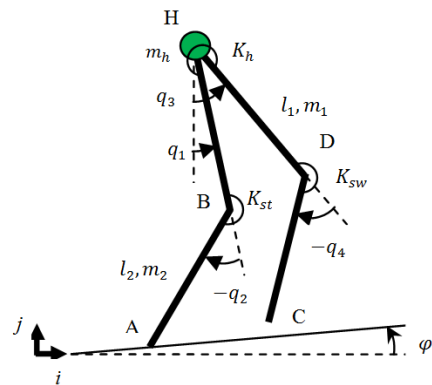


Figure 2. Stance phase generalized coordinates and (b) Flight phase generalized coordinates for the kneed biped

Parameter	Value (SI units)	Description
m_1, l_1, \bar{I}_1	8, 0.45, 0.135	Mass, length and moment of inertia of thigh BH, DH
m_2, l_2, \bar{I}_2	7, 0.5, 0.146	Mass, length and moment of inertia of shank AB, CD
m_h	50	Point mass of the hip at H
φ	arbitrary	Terrain slope with respect to the horizon
u_1	variable	Torque of the hip motor in the direction of $q_3 - q_1$
u_2	variable	Torque of the motor in knee B in the direction of q_2
u_3	variable	Torque of the motor in knee C in the direction of q_4
K_h	200	Torsion spring stiffness in the hip
K_{st}	1000	Torsion spring stiffness in the knee of the stance leg
K_{sw}	500	Torsion spring stiffness in the knee of the swing leg

Table 2. Nomenclature of the kneed biped robot

By defining the stance phase state vector as $\mathbf{x}_s = [\mathbf{q}_s; \dot{\mathbf{q}}_s]$, the dynamic equations become first-order state equations. By defining the flight phase generalized coordinates as $\mathbf{q}_f = [q_1, q_2, q_3, q_4, x_h, y_h]^T$, the dynamic equations of the flight phase become:

$$[\mathbf{D}_f(\mathbf{q}_f)]_{6 \times 6} \cdot [\ddot{\mathbf{q}}_f]_{6 \times 1} + [\mathbf{C}_f(\mathbf{q}_f, \dot{\mathbf{q}}_f)]_{6 \times 1} = [\mathbf{B}_f]_{6 \times 3} \cdot [\mathbf{u}_f]_{3 \times 1} \quad (11)$$

We use Lagrange's impact model to find the collision map in touch-down:

$$\mathbf{D}_f(\mathbf{q}_f) \cdot (\dot{\mathbf{q}}_f^+ - \dot{\mathbf{q}}_f^-) = \hat{\mathbf{Q}} \quad (12)$$

in which D is the inertia matrix:

$$\mathbf{T} = \frac{1}{2} \dot{\mathbf{q}}_f^T \mathbf{D}_f(\mathbf{q}_f) \dot{\mathbf{q}}_f \quad (13)$$

The principle of virtual work provides generalized impact modelling. In the following equations, q_i denotes the i -th component of \mathbf{q}_f . The position of the touch-down foot in terms of flight coordinates is:

$$x_C = q_5 + l_1 \sin q_3 - l_2 \sin(-q_3 - q_4) \quad (14)$$

$$y_C = q_6 - l_1 \cos q_3 - l_2 \cos(-q_3 - q_4) \quad (15)$$

and virtual work is denoted:

$$\delta W = \hat{F}_x \cdot \delta x_C + \hat{F}_y \cdot \delta y_C = \sum_{i=1}^4 \left(\hat{F}_x \frac{\partial x_C}{\partial q_i} + \hat{F}_y \frac{\partial y_C}{\partial q_i} \right) \delta q_i \equiv \sum_{i=1}^4 \hat{Q}_i \delta q_i \quad (16)$$

So, the generalized impacts become:

$$\hat{Q}_i = \hat{F}_x \frac{\partial x_C}{\partial q_i} + \hat{F}_y \frac{\partial y_C}{\partial q_i} \quad (17)$$

After touch-down, we change the notation for labelling the feet, which gives us 8 equations in terms of pre-contact and post-contact coordinates and velocities.

Assuming fully plastic contact, the post-contact position of the hip produced by differentiating the post-contact stance coordinates is:

$$\begin{bmatrix} \dot{q}_{f5}^+ \\ \dot{q}_{f6}^+ \end{bmatrix} = \begin{bmatrix} \dot{x}_h(\mathbf{q}_s^+, \dot{\mathbf{q}}_s^+) \\ \dot{y}_h(\mathbf{q}_s^+, \dot{\mathbf{q}}_s^+) \end{bmatrix} \quad (18)$$

Equations (12,18) and the 8 equations contain 16 equations with 16 unknowns $\dot{\mathbf{q}}_f^+, \mathbf{q}_s^+, \dot{\mathbf{q}}_s^+, \hat{F}_x, \hat{F}_y$, which constitute the touch-down map. These equations, together with the stance and flight phase and take-off map, form the hybrid dynamic model.

3. Gait Generation

3.1. Straight-legged biped

For simplicity and to compare the results with [23], we assume massless feet and place the leg masses at points C and D. The only event that should dissipate (significant) energy during a running cycle is touch-down. However, massless feet make it possible to touch down without energy losses, resulting in passive periodic orbits. Thus, *gait generation* will consist of finding a set of initial conditions and control commands that can produce a periodic orbit for running. A Poincare map of one complete running step will serve as a convenient method of describing a periodic orbit. A complete running step includes stance phase, take-off, a flight phase and touch-down. We choose the post-contact state vector as the Poincare section, which is also the initial condition of the stance phase. Thus, the state vector at the beginning of a stance phase gives the Poincare map its input, and it outputs the next state vector at the beginning of the next stance phase (the next step). Although \mathbf{x}_s has six components, at the very beginning of the stance phase the spring starts at zero compression and the initial length of the leg is the same every time, such that our Poincare map state vector \mathbf{x} consists of a five-dimensional vector.

We begin by finding a *passive* solution, where the torque at the hip remains zero at all times. The Poincare map for a passive gait is:

$$\mathbf{x}(k+1) = \mathbf{P}(\mathbf{x}(k)). \quad (19)$$

in which k is the number of steps. Any fixed point of the Poincare map indicates a periodic orbit of the overall dynamic model and provides a valid initial condition for a passive periodic running gait. To find the fixed point of the Poincare map, find the zero of the function:

$$Er = \mathbf{x}(k+1) - \mathbf{x}(k) \quad (20)$$

Specifically, numerical optimization methods can find a solution that minimizes the 2-norm of (11). The fixed point of the map is:

$$\mathbf{x}^* = \mathbf{P}(\mathbf{x}^*). \quad (21)$$

At least one fixed point exists for any given running speed. We measure the running speed as the horizontal velocity of the CoM at the touch-down instance, and then add its difference from the desired velocity to the norm of the error function in the optimization routine.

A gait designed for an uphill run will require torques (i.e., an *active* gait). Moreover, we shall see that active gaits may also provide a better starting point (linearization) for our closed-loop control strategy. To find such active running gaits, we find a fixed point of the active Poincare map:

$$\mathbf{x}(k+1) = \mathbf{P}(\mathbf{x}(k), \mathbf{U}(k)) \quad (22)$$

Vector \mathbf{U} contains the data of the control effort of one step. Since we wish to use discrete-time control methods, we require controls to be constant over discrete-time intervals. We use one constant motor torque during each phase (i.e., a constant value in stance and a different constant value in flight). Since the system has only one (hip) motor, the control vector for this biped model consists of a two-dimensional vector:

$$\mathbf{U} = [u_s; u_f]. \quad (23)$$

The active fixed point is:

$$\begin{bmatrix} \mathbf{x}^* \\ \mathbf{U}^* \end{bmatrix}_{5 \times 1} = \mathbf{P} \left(\begin{bmatrix} \mathbf{x}^* \\ \mathbf{U}^* \end{bmatrix}_{5 \times 1}, \begin{bmatrix} \mathbf{U}^* \end{bmatrix}_{2 \times 1} \right). \quad (24)$$

3.2. Kneel biped

Because the feet have mass in this model, no passive running gait exists on horizontal terrain. Again, the post contact state vector becomes a Poincare section. An active fixed point of the Poincare map:

$$\begin{bmatrix} \mathbf{x}^* \\ \mathbf{U}^* \end{bmatrix}_{8 \times 1} = \mathbf{P} \left(\begin{bmatrix} \mathbf{x}^* \\ \mathbf{U}^* \end{bmatrix}_{8 \times 1}, \begin{bmatrix} \mathbf{U}^* \end{bmatrix}_{6 \times 1} \right) \quad (25)$$

will help generate gaits on horizontal or sloped terrains. Three motors provide torque - one in the hip and two in the knees. Again, the motor torques remain constant during each continuous time phase and, therefore, vector \mathbf{U} has three components for the stance phase and three for the flight.

Countless fixed points exist, each corresponding to a running speed. We find a fixed point that minimizes energy expenditure subject to the constraint of the swing leg remaining clear of the ground. The energy expenditure index will be introduced in the next section.

3.3. Cost of transport

Assuming the 100% efficiency of the motors, the energy expenditure in one step is calculated:

$$W = \sum_{i=1}^3 \int_0^{t_{step}} |\dot{\theta}_i u_i| dt \quad (26)$$

in which u_i denotes the motor torque of each joint, $\dot{\theta}_i$ is the angular velocity of the corresponding joint in the direction of u_i , and t_{step} defines the time interval of one step of the gait.

The *cost of transport* (COT) - i.e., the consumed energy per total weight per distance travelled - provides a useful measure for energy expenditure comparisons:

$$COT = \frac{W}{m_{tot} g \sqrt{L_s^2 + h_s^2}} \quad (27)$$

in which L_s and h_s are the horizontal and vertical components of the stride, respectively [26].

4. Stabilizing Controller

The passive and active open-loop gaits found in the previous section are unstable; even tiny disturbances, like those due to truncated numerical calculations in simulations, will cause the joint trajectories to drift and result in the robot falling after a few steps. To investigate gait stability, consider the linearized Poincare map around the fixed point (26) or (27) as:

$$(\mathbf{x}(k+1) - \mathbf{x}^*) = \mathbf{A} \cdot (\mathbf{x}(k) - \mathbf{x}^*) + \mathbf{B} \cdot (\mathbf{U}(k) - \mathbf{U}^*) \quad (28)$$

in which $[\mathbf{A}]_{n \times n}$ and $[\mathbf{B}]_{n \times m}$ are coefficient matrices obtained by linearization, where $n=5$ and $m=2$ for the straight leg biped and $n=8$ and $m=6$ for the kneel biped. Note that for the passive gait $\mathbf{U}^* = [0; 0]$. We rewrite equation (30) as:

$$\delta \mathbf{x}(k+1) = \mathbf{A} \delta \mathbf{x}(k) + \mathbf{B} \delta \mathbf{U}(k). \quad (29)$$

Now, instead of a hybrid nonlinear dynamic system (2, 4, 5, 6-9), we have a linear digital system (31) with an equilibrium point at the origin. This system will be stable, if all of the eigenvalues of matrix \mathbf{A} are located inside the unit circle. A state feedback control:

$$\delta \mathbf{U}(k) = -\mathbf{K} \delta \mathbf{x}(k). \quad (30)$$

stabilizes system (31). Linear control techniques can produce an appropriate control gain matrix \mathbf{K} . In pole placement, the poles of a closed-loop system $\mathbf{A}-\mathbf{BK}$ are simply placed inside the unit circle. With the discrete linear quadratic regulator (DLQR) method, a matrix \mathbf{K} is found that minimizes the cost function:

$$J = \sum \left(\delta \mathbf{x}(k)^T \mathbf{Q} \delta \mathbf{x}(k) + \delta \mathbf{U}(k)^T \mathbf{R} \delta \mathbf{U}(k) \right) \quad (31)$$

5. Results: Straight Leg Biped

The nonlinear optimization needed to minimize (22) presents some practical difficulties. Since this complicated function contains the hybrid dynamic model with continuous and discontinuous time phases, in practice the optimization algorithm will often settle in a local minimum. To solve this problem, after finding each solution we re-initialize the optimization algorithm by rounding the last result, and repeat this procedure until reaching the desired tolerance. The presence of events in the dynamic model causes challenges in choosing an integration step size; we use a relatively large time step, with a maximum step size of 10 ms for the continuous-time phases, but a much smaller time step around the events, with the maximum step size in the order of 0.1 ms.

The phase diagram of leg AH for five steps of open loop passive running with a speed of 0.85 m/s is shown in Figure 3, in which point P is the start point, curve PQ corresponds to the stance leg, QR to flight, RS to the swing leg and SP to flight. Qualitatively speaking, its overall shape appears to be in agreement with the results in [23] for a simple biped model with only three point masses. Note that this passive limit cycle is unstable; the phase diagram diverges due to the (disturbance) error accumulation in numerical calculations, causing the biped model to fall down after running five steps (the red line exiting to the left in Figure 4b). Considering that points P and R correspond to the touch-downs in the limit cycle of Figure 3, one can see that there is no discontinuity in the velocities; therefore, in this gait touch-down occurs with no energy losses. However, in the last step before failure, point P changes to a vertical line with an instantaneous velocity change in touch-down, which causes energy dissipation. This small vertical line is recognizable in the figure by a blue point just beneath the red point in P. An

energy-conserving touch-down occurs for biped models with massless springy feet when the velocity of the touch-down foot is in the direction of the touch-down leg [23]. This condition has been satisfied automatically because the calculated fixed point is passive and energy conserving. However, energy dissipation is inevitable at touch-down with biped robots with foot mass. The thick lines in Figure 5 representing this gait show that the total mechanical energy of the robot remains constant during the gait, serving to verify the validity of our dynamic equations and their solutions.

The stick diagram of the resulting actuated (non-passive) gait running up a slope angle of $\varphi = 5^\circ$ and a horizontal velocity of 0.85 m/s is shown in Figure 4. For points P and R in this figure, the superscript '-' represents the pre-contact state and '+' represents post-contact. Note the discontinuities in velocities with resulting energy losses at touch-down. Due to the uphill motion, the total mechanical energy of the robot increases with each step (Figure 5, thin lines). Figure 6 shows the control effort for the generated gait, remaining constant in each phase. The COT for running gaits increases with the terrain incline in a linear manner (Figure 8).

The maximum eigenvalue of matrix \mathbf{A} corresponding to the passive gait on horizontal terrain is 13.8, and for the active gait on 5° sloped terrain is $5.8+2.7i$. So, although both of these gaits are unstable, the magnitudes of the eigenvalues are small enough that stabilization using discrete-time state feedback control constitutes a viable strategy.

By choosing a large constant of $q = 4000$ and $Q = q I$, along with a small constant $r = 1$ and $R=r I$, we design feedback controls for the two generated gaits. For the passive gait, the maximum closed-loop pole became 0.49 and for the active gait 0.59. This controller stabilizes the fixed points and the robot model displays a steady and hybrid dynamic model of both of the gaits around their stable running motion with the designed velocity.

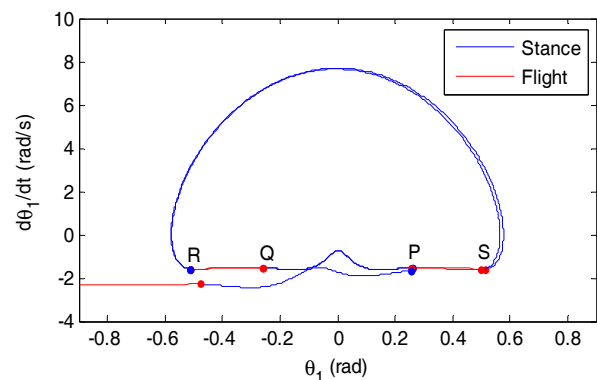


Figure 3. Phase diagram of leg AH of the straight leg biped model with an unstable passive running gait on horizontal terrain, starting from the fixed point

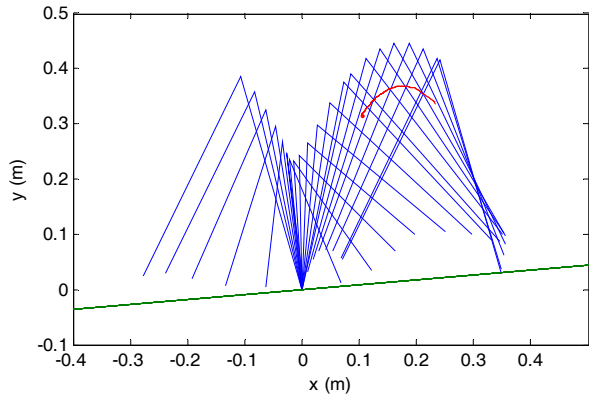


Figure 4. Stick diagram of one step of running on 5° sloped terrain with a velocity of 0.85 m/s and 30 ms time intervals between snapshots

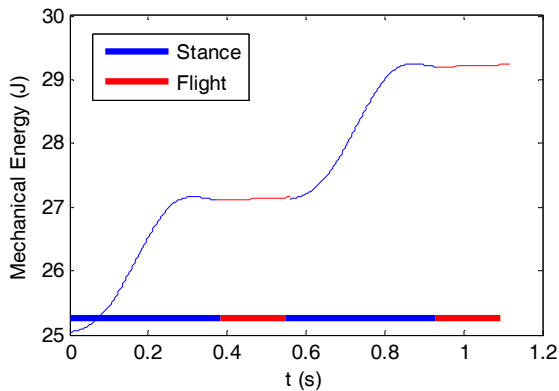


Figure 5. Total mechanical energy of the robot for two steps of running (thick line for horizontal and thin line for sloped terrain)

Figure 8 and 10 show convergence with the limit cycles using control law (30), and Figure 9 and 11 show their control efforts, which approach the fixed point values of the gait and reach a steady state after about 15 steps. The shape of the passive limit cycle for running on horizontal terrain in Figure 8 is similar to the limit cycle of a biped model with three point masses and without legs inertias in [23], because both of the models have massless springy feet. Moreover, for both models the closed-loop control effort converges on zero as the system converges on a passive gait (Figure 9). The active running gait on sloped terrain has a different shaped limit cycle (Figure 10), which also has energy dissipation at touch-down (green line), and the control effort converges on the non-zero torque values of the active fixed point (Figure 11).

It is desirable that there are small deviations of motor torques from the fixed point values. In these simulations, each component of the initial condition state vector is 1% deviated from the fixed point vector for the gait on horizontal terrain and 3% for sloped terrain. More deviations lead to divergence from the limit cycle and failure.

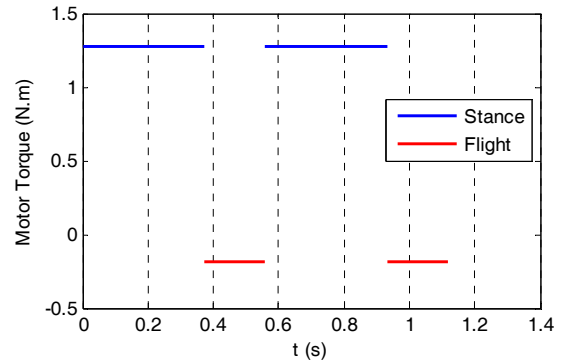


Figure 6. Control effort for a two-step of running gait on 5° sloped terrain which is constant during each phase

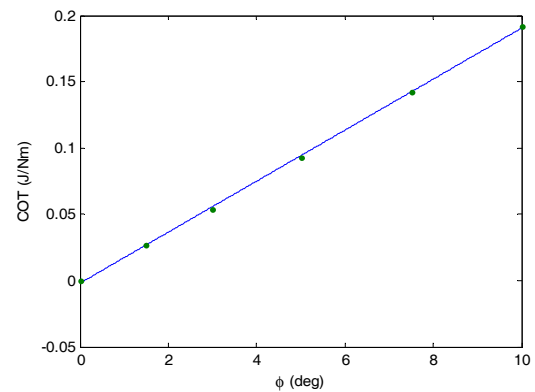


Figure 7. Cost of transport vs. terrain slope for the straight leg robot

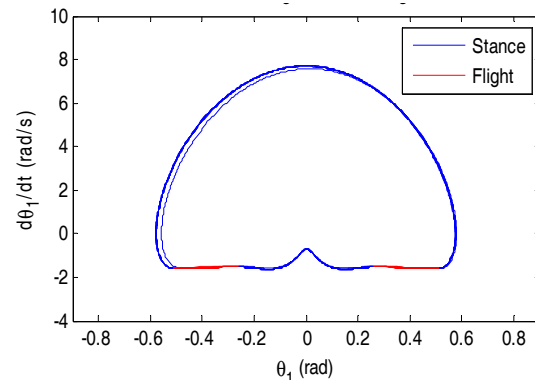


Figure 8. Phase diagram of leg AH₁, starting from an initial state deviated from the fixed point

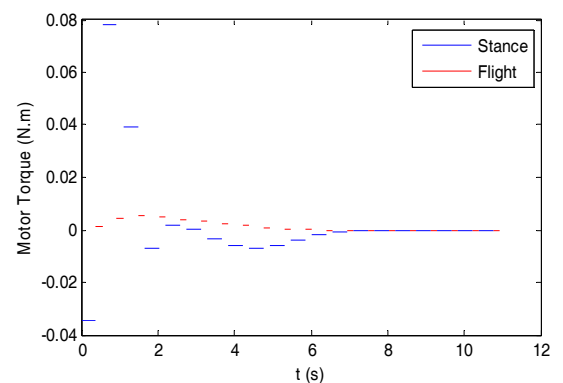


Figure 9. Control effort for 20 steps of closed-loop running on horizontal terrain

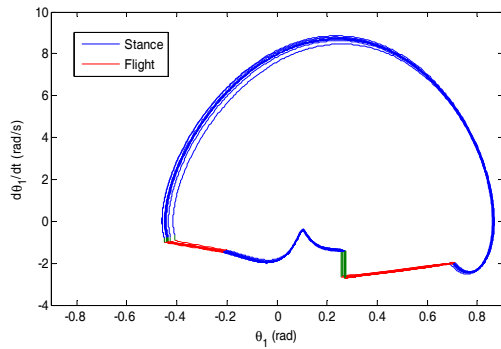


Figure 10. Phase diagram of leg AH for 20 steps, starting from an initial state deviated from the fixed point

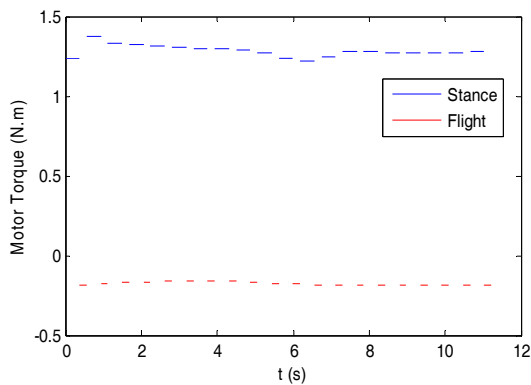


Figure 11. Control effort for 20 steps of closed-loop running on 5° sloped terrain

6. Results: Kneed Biped

To generate an efficient running gait, the springs' rates should be adjusted for that speed. We found a set of values by trial and error that can produce a natural-looking gait with a speed of 10 m/s when compared to the fastest human running speed of 12.4 m/s [28]. A stick diagram of the generated gait on sloped terrain with an angle of 5° appears in Figure 12. The red curves indicate the trajectory of the CoM during flight, demonstrating a considerable range in flight. Although unstable, these gaits can continue open-loop running for about nine steps before falling down, appearing to have better stability characteristics than the telescoping leg biped model. The linearized Poincare map (31) for the gait on horizontal terrain has a maximum eigenvalue of 2.92 and for sloped terrain 3.63, quite suitable for the application of a linear state feedback controller (compared to 13.8 for the prismatic springy leg model). The use of the DLQR method produces matrix $[K]_{6 \times 8}$ and the control law (32) places the closed-loop maximum poles of the systems at 0.4034 and $0.333 + 0.182i$ for horizontal and sloped terrains respectively. This control law stabilizes the nonlinear hybrid system and generates a stable periodic running motion. When the initial condition is coincident with the fixed point of the Poincare map, the phase diagram of the closed-loop system remains on the limit cycle. Perturbing each element of the starting state by 2% from the fixed point, we observe initial deviations of the phase from the

limit cycle with ultimate convergence within five steps (Figure 14 and Figure 16 for the horizontal and sloped terrains respectively). If we perturb only one component of the initial state vector by 10%, the closed-loop system will converge on the limit cycle as well (larger perturbations cause divergence in both cases). The figures demonstrate a local basin of attraction. The vertical green lines P and R correspond to touch-down with instantaneous velocity changes. Notice that the gait on the slope has a greater velocity discontinuity and larger energy losses than the horizontal gait. Furthermore, Figure 15 and Figure 17 show that bigger torque magnitudes are needed on the sloped terrain. Due to the disturbance in the initial conditions, the control torques have some fluctuations and converge on U^* after a few steps. These torques remain constant during each stance and flight phase (labelled in accordance with Table 2).

In Figures 7 and 13, the dots show the values of the computed COT for the generated gaits on different terrain slopes, and a line is fitted to them. The generated running gait on level ground results in a cost of transport of 1.98 and increases with the slope of the terrain. Comparing the two figures, we conclude that the kneed biped model requires much larger COTs than the straight leg model – due to the fact that the straight leg biped model had conceptual massless springy feet and its gait was passivity-based. However, our kneed model presents

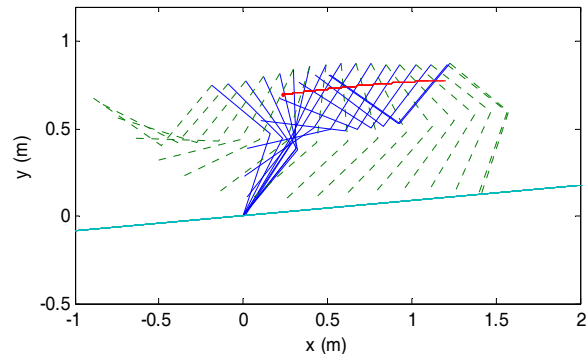


Figure 12. Stick diagram of one step of running with a velocity of 10 m/s and 10 ms time intervals between snapshots, (a) on horizontal terrain (b) on 5° sloped terrain

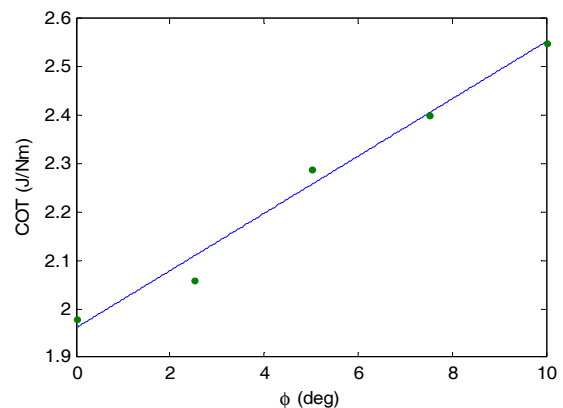


Figure 13. Cost of transport vs. terrain slope for the kneed leg robot

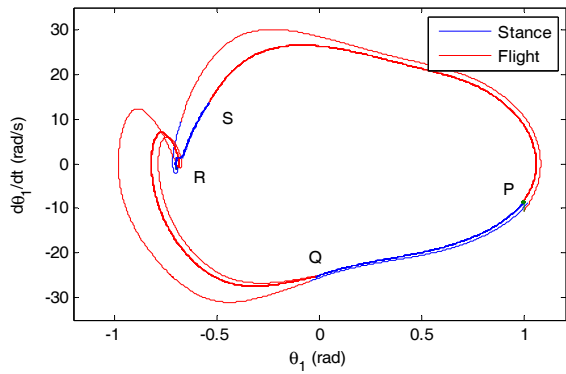


Figure 14. Phase diagram of leg BH, starting from an initial state deviated from the fixed point

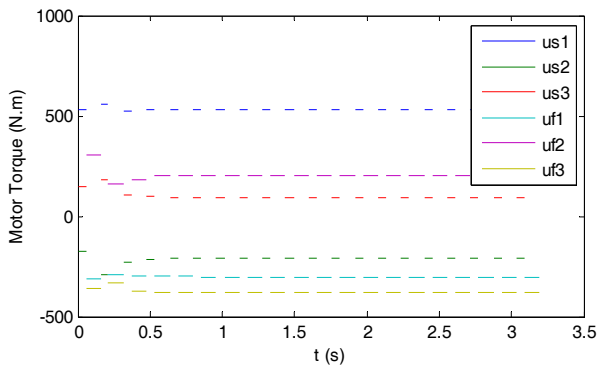


Figure 15. Control effort for 20 steps of closed-loop running on horizontal terrain

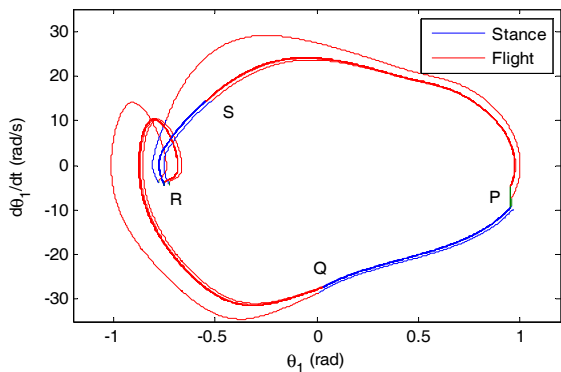


Figure 16. Phase diagram of leg BH for ten steps, starting from an initial state deviated from the fixed point

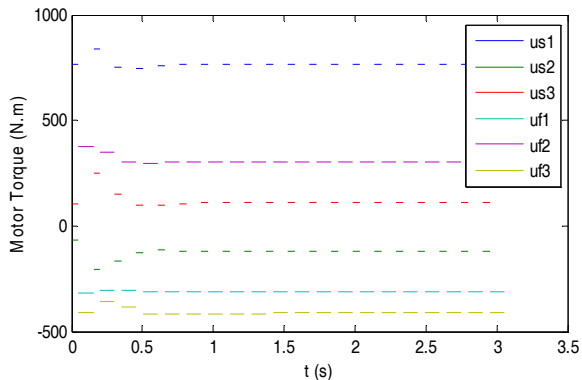


Figure 17. Control effort for 20 steps of closed-loop stable running on 5° sloped terrain

a more realistic model, similar to a human leg structure. In the next section we will show that the cost of transport can be reduced with variable control torques during phases. In addition, note that the obtained COT points do not lie on a straight line in Figure 13, as in Figure 7; the straight leg model has only one motor in the hip and assuming a constant torque for it causes a unique gait for each slope and each velocity, whereas the kneed biped with three motors does not have a unique gait for each condition (we find that with minimum energy consumption).

7. Further Control Input Discretization

In the controller (30) for the linear system (29) investigated in the previous sections, the torques were constant during each stance and each flight phase; reducing the number of calculations needed yet restricting the energy efficiency of the gait. In this section, the control method is generalized for running gaits with variable motor torques to show the generality of the control strategy. Here, the motor torques are discretized into smaller time steps, but remain constant during each step. Due to the variation of motor torques, the stance and flight times will vary, requiring us to choose a number of steps that cover more time than the entire phase. Looking at the stance time interval 0.056 s and the flight time interval 0.104 s from the previous section, we choose a stance time step size of 0.02 s and a flight time step size of 0.04 s, with 4 time steps for each phase. The control vector is defined as:

$$U = [u_{s1,1}, u_{s2,1}, u_{s3,1}, \dots, u_{s1,n}, u_{s2,n}, u_{s3,n}, u_{f1,1}, u_{f2,1}, u_{f3,1}, \dots, u_{f1,m}, u_{f2,m}, u_{f3,m}] \quad (32)$$

such that it contains all the motor torque values for both the stance and the flight phase of one step. In this formula, s and f indicate the stance and flight phases, 3 is the number of motors of the robot and n and m are the number of the discretization of the stance and flight phases, respectively. Thus, the active fixed point similar to (27) has $[x^*]_{8 \times 1}$ and $[U^*]_{3(m+n) \times 1}$. To find the fixed point, an optimization problem with $(8+3mn)$ parameters produces a minimum COT, constrained by $x(k+1) = x(k)$ and the clearance of the swing leg. In this manner, any active biped running gait can be formulated and stabilized using this control strategy. The generated gait results in a cost of transport of 1.47 J/Nm. We repeat the optimization procedure with a stance time step size of 0.01 s and a flight time step size of 0.02 s, for which the cost of transport of the generated gait is 1.31J/Nm. The motor torques for one step of these gaits is shown in Figure 18b and c compared to the results for constant torque gait in Figure 18a. The use of smaller time steps has reduced the maximum torque required. Moreover, the COT decreases with increasing step size in an almost linear manner (Figure 19). The generated

energy-efficient running gait with variable motor torques with a stance and flight time step size of 0.01 s and 0.02 s is shown in Figure 20. This gait has a stance phase time interval of 0.057 and of flight of 0.121 s. The COTs of different biped models and gaits are summarized in Table 3. Guo et al. [7] generated a biped running gait with a COT of 1.01 J/Nm using a rigid model with feet, knees and a torso and six motors in the ankles, knees and hip joints. This more efficient gate may be due to the existence of more degrees of actuation or the better performance of their optimization procedure. We use the MATLAB `fmincon` tool to find the fixed point and minimize the energy consumption. This optimization procedure with 56 parameters requires extensive calculations and is likely to settle in a local minimum. Although it does not guarantee a global minimum, we did show our controller’s applicability to stabilizing other biped running gaits that have been generated by a global optimization, for example in [27] and [30]. To stabilize those gaits, their variable torque profiles should be discretized as (32) to use the control law (30).

To test the control algorithm we use a gait with 0.01 s stance time step size. Again the Poincare Map is linearized around the fixed point and with the control law of (32) for the linear discrete system (31), and matrix $[K]_{3(m+n) \times 8}$ is found using DLQR method. Controller (32), when applied to the main system, generates control command for one step using the feedback of stance state in the post contact instance. Starting from a state 6% disturbed from the fixed point, the phase diagram of one leg of closed-loop running for 20 steps is shown in Figure 21 which shows convergence on a steady stable gait, and the control effort for ten steps is depicted in Figure 22.

The maximum deviation of the initial conditions from the fixed point for which the controller of constant torque gait converges on the limit cycle is 2% while it is 6% for the gait with variable torque. So, the variable torque has the advantages of lower COT and better controllability, while its drawback is that it needs a greater number of calculations to find the fixed point and it can be more difficult to implement on a real robot than the event-based controller.

Biped robot	Horizontal terrain	5° sloped terrain
Straight leg biped	0	0.092
Kneed biped with constant torques	1.98	2.29
Kneed biped with variable torques	1.31	-
Kneed fully actuated biped with variable torques [7]	1.01	-

Table 3. Cost of transport of different running biped models

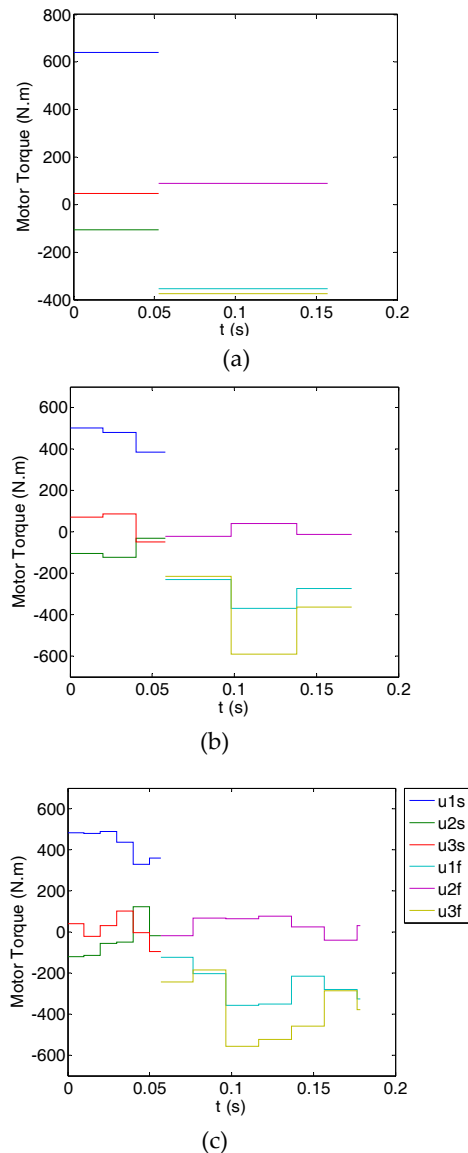


Figure 18. (a) Control effort of one step of running on horizontal terrain with constant torques, COT = 1.98, (b) variable torques with 0.02 s and 0.04 s time steps for stance and flight, COT = 1.47, and (c) variable torques with 0.01 s and 0.02 s time steps for stance and flight, COT = 1.31.

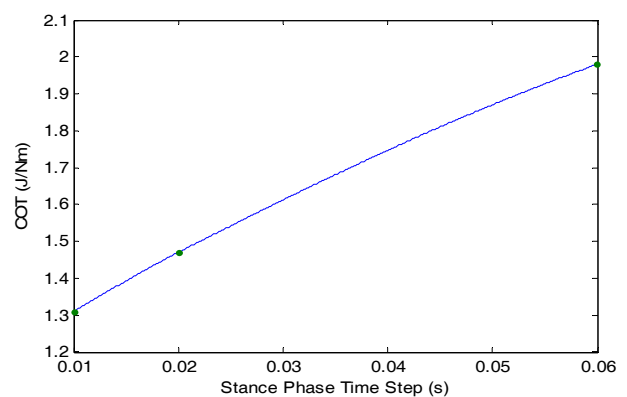


Figure 19. Cost of transport vs. time step size in a variable torque gait

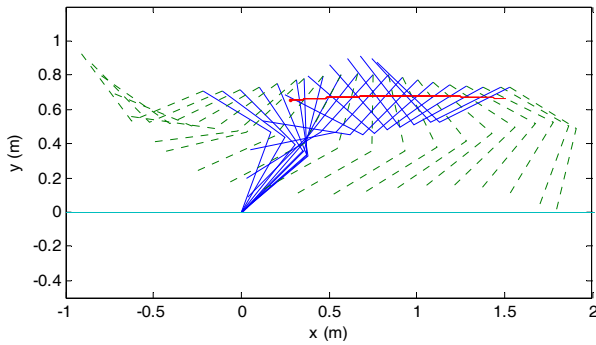


Figure 20. Stick diagram of one step of running with variable motor torques on horizontal terrain

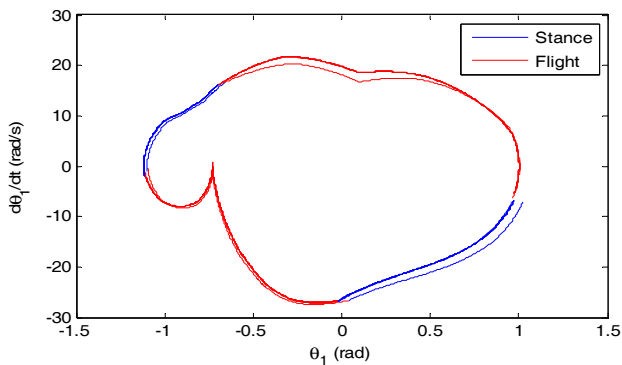


Figure 21. Phase diagram of leg BH for 20 steps of closed-loop stable running on horizontal terrain with variable torques, starting from a point deviated 6% from the fixed point

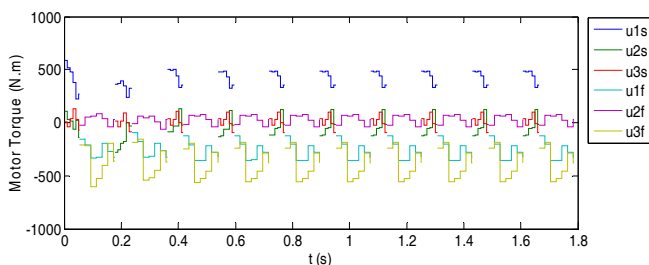


Figure 22. Control effort for ten steps of closed-loop running on horizontal terrain

8. Conclusion and Discussion

The dynamic equations of biped robot running were formulated and a numerical framework was proposed to derive and solve the equations for various biped models. It was shown that the proposed compliant kneed multi-body biped model can produce active running limit cycles with either constant or variable motor torques during each phase. This model has a variable stiffness – changing between flight and stance – for greater energy efficiency. A fixed point of a single-step Poincare map provided the basis to generate periodic running gaits. A discrete-time linear state feedback controller stabilized the linearized Poincare map around the fixed point. Simulations demonstrated that the controller can stabilize both telescoping-leg and kneed-leg models, on both

horizontal and inclined surfaces. The limit cycles and the control command for the telescoping leg biped are qualitatively in agreement with the passive limit cycles in [23]. Our running gaits are not limited to passive gaits like in [19], [22] and [23], and our controller, being able to stabilize both passive and active running gaits, is much simpler than HZD [21] for active gaits. The HZD controller is a hybrid, with continuous-time feedback signals applied in stance and flight phases, and with discrete updates of controller parameters performed at the transitions between phases, while our controller is event-based, with just updates at the instance of post-touch-down. The HZD controllers are designed separately for the stance and flight phases so that the restricted Poincare map is stable, but our controller is calculated for the entire step using the linearized Poincare map around its active fixed point. After applying the controller to running gaits with constant motor torques during each (stance and flight) phase, in section 7 the motor torques were discretized using smaller intervals to show the generality of this controller. The controller formulation in section 7 should be able to stabilize any active biped running gait with variable discretized motor torques. Using more discretizations requires significantly more calculations to find the fixed point, but the controller consumes less energy.

9. Acknowledgments

We thank Mr S. J. Hasaneini for his useful comments.

10. References

- [1] Y. Hurmuzlua, F. Genot and B. Brogliato (2004) Modeling, stability and control of biped robots - a general framework, *Automatica*, vol. 40, pp. 1647–1664.
- [2] T. McGeer (1993) Dynamics and control of bipedal locomotion, *Journal of Theoretical Biology*, vol. 166, no. 3, pp. 277–314.
- [3] A. Goswami, B. Thuilot and B. Espiau (1998) A study of the passive gait of a compass-like biped robot: Symmetry and chaos, *International Journal of Robotics Research*, vol. 17, no. 12, pp. 1282–1301.
- [4] S. H. Collins, M. Wisse, and A. Ruina (2001) A three-dimensional passive dynamic walking robot with two legs and knees, *International Journal of Robotics Research*, vol. 20, no. 7, pp. 607–15.
- [5] D. Owaki, M. Koyama, S. Yamaguchi, S. Kubo and A. Ishiguro (2010) A Two-dimensional passive dynamic running biped with knees, *IEEE International Conference on Robotics and Automation (ICRA)*, Alaska, pp. 5237 - 5242.
- [6] A. Vleugels (2011) Famous ASIMO robot gets upgraded, *United Academics Magazine*, November 10.
- [7] Q. Guo, C. J. B. Macnab and J. K. Pieper (2010) Generating efficient rigid biped running gaits with calculated take-off velocities, *Robotica*, Vol. 29, No. 04, pp. 627-640.

- [8] S. Kajita, F. Kanehiro, K. Kaneko, K. Fujiwara, K. Yokoi and H. Hirukawa (2002) A realtime pattern generator for biped walking, In Proc. of the 2002 IEEE International Conference on Robotics and Automation, Washington, D.C., pp. 31-37.
- [9] R. Blickhan (1989) The spring-mass model for running and hopping, *J. Biomech*, vol. 22, pp. 1217-1227.
- [10] H. Geyer, A. Seyfarth and R. Blickhan (2006) Compliant leg behavior explains basic dynamics of walking and running, *Proceedings Biological sciences / The Royal Society*, vol. 273, pp. 2861-7.
- [11] J. Rummel, F. Iida and A. Seyfarth (2006) One-Legged Locomotion with a Compliant Passive Joint, *Proceedings of the 9th International Conference on Intelligent Autonomous Systems*, Tokyo, T. Arai et al. (Eds.), IOS Press, 566-573.
- [12] F. Iida, J. Rummel and A. Seyfarth (2008) Bipedal walking and running with spring-like biarticular muscles, *Journal of biomechanics*, vol. 41, pp. 656-67.
- [13] J.C. Dean and A. D. Kuo (2009) Elastic coupling of limb joints enables faster bipedal walking, *Journal of the Royal Society, Interface / the Royal Society*, vol. 6, pp. 561-73.
- [14] B. Verrelst, B. Vanderborght, J. Vermeulen, R. Ham, J. Naudet and D. Lefeber (2005) Control architecture for the pneumatically actuated dynamic walking biped "Lucy", *Mechatronics*, vol. 15, pp. 703-729.
- [15] K. Hosoda, T. Takuma, A. Nakamoto and S. Hayashi (2008) Biped robot design powered by antagonistic pneumatic actuators for multi-modal locomotion, *Robotics and Autonomous Systems*, vol. 56, pp. 46-53.
- [16] J. Pratt and B. Krupp (2008) Design of a bipedal walking robot, *Proceedings of SPIE*, vol. 6962.
- [17] K. Radkhah, T. Lens, A. Seyfarth and O. von Stryk (2010) On the influence of elastic actuation and monoarticular structures in biologically inspired bipedal robots, 3rd IEEE RAS & EMBS International Conference on Biomedical Robotics and Biomechatronics.
- [18] Z. You and Z. Zhang (2011) An overview of the underactuated biped robots, *Proceeding of the IEEE International Conference on Information and Automation Shenzhen, China*.
- [19] T. McGeer (1990) Passive Bipedal running, *Proc. Roy. Soc. London*, vol. 240, no. 1297, pp. 107-134.
- [20] Jesse W. Grizzle, Gabriel Abba and Franck Plestan (2001) Asymptotically Stable Walking for Biped Robots: Analysis via Systems with Impulse Effects, *IEEE Transactions on Automatic Control*, vol.46, no.1.
- [21] C. Chevallereau, E. R. Westervelt and J. W. Grizzle (2005) Asymptotically Stable Running for a Five-Link, Four-Actuator, Planar Bipedal Robot, *International Journal of Robotics Research*, vol. 24, iss. 6.
- [22] S. H. Hyon and T. Emura (2004) Running Control of a Planar Biped Robot Based on Energy-Preserving Strategy, *Proceedings of IEEE International Conference on Robotics and Automation*, New Orleans, USA.
- [23] Y. Hu, G. Yan and Z. Lin (2010) Stable running of a planar underactuated biped robot, *Robotica*, pp. 1-9.
- [24] S. W. Lipfert (2010) Kinematic and Dynamic Similarities between Walking and Running, Hamburg: Verlag Dr. Kovac, ISBN-10: 3830050305 .
- [25] B.M. Nigg, W. Liu (1999) The effect of muscle stiffness and damping on simulated impact force peaks during running, *Journal of Biomechanics*, vol. 32, iss. 8 , pp. 849-856.
- [26] S. Collins, A. Ruina, R. Tedrake and M. Wisse (2005) Efficient bipedal robots based on passive-dynamic walkers, *Science*, vol. 307, no. 5712, pp. 1082-1085.
- [27] S. J. Hasaneini, C. J. B. Macnab, J. E. A. Bertram and H. Leung (2013) The dynamic optimization approach to locomotion dynamics: human-like gaits from a minimally-constrained biped model, *Journal of Advanced Robotics*, in press.
- [28] Joggers United (2012) 40 Random Facts about Running and Runners, February 23, 2012.
- [29] E. R. Westervelt, J. W. Grizzle, C. Chevallereau, J. H. Choi and B. Morris (2007) Feedback control of dynamic bipedal robot locomotion, CRC Press, Boca Raton.
- [30] C. Chevallereau and Y. Aoustin (2001) Optimal reference trajectories for walking and running of a biped robot, *Robotica*, vol. 19, no. 5, pp. 557-569.